

Location recognition over large time lags

*Original*

Location recognition over large time lags / Fernando, B., Tommasi, T., Tuytelaars, T.. - In: COMPUTER VISION AND IMAGE UNDERSTANDING. - ISSN 1077-3142. - ELETTRONICO. - 139:(2015), pp. 21-28. [10.1016/j.cviu.2015.05.016]

*Availability:*

This version is available at: 11583/2726166 since: 2019-02-25T01:22:52Z

*Publisher:*

Elsevier

*Published*

DOI:10.1016/j.cviu.2015.05.016

*Terms of use:*

This article is made available under terms and conditions as specified in the corresponding bibliographic description in the repository

*Publisher copyright*

Elsevier postprint/Author's Accepted Manuscript

© 2015. This manuscript version is made available under the CC-BY-NC-ND 4.0 license  
<http://creativecommons.org/licenses/by-nc-nd/4.0/>. The final authenticated version is available online at:  
<http://dx.doi.org/10.1016/j.cviu.2015.05.016>

(Article begins on next page)

# Location Recognition Over Large Time Lags

Basura Fernando\*, Tatiana Tommasi, Tinne Tuytelaars

*KU Leuven ESAT-PSI, iMinds  
Kasteelpark Arenberg 10 - bus 2441  
B-3001 Heverlee, Belgium*

## Abstract

Would it be possible to automatically associate ancient pictures to modern ones and create fancy cultural heritage city maps? We introduce here the task of recognizing the location depicted in an old photo given modern annotated images collected from the Internet. We present an extensive analysis on different features, looking for the most discriminative and most robust to the image variability induced by large time lags. Moreover, we show that the described task benefits from domain adaptation.

*Keywords:* location recognition, cross-domain image retrieval, domain adaptation

## 1. Introduction

A hundred year old photograph or a postcard can reveal a lot about our culture and history. Following this idea, many cultural heritage campaigns recently started to promote the digitization of large amounts of visual data. Several cities and towns all over the world, as well as institutions such as universities or museums, are bringing archives with their images and footage online, providing public access and calling for methods to efficiently open up and exploit these resources [1, 2].

At the time when photography was not affordable for private and everyday use, most of the pictures were taken in public places and depict buildings, monuments, statues, or more in general, common locations of interest. Some of those are landmarks and tourist attractions. Others are locations with historical value. Popular landmarks often appear in modern digital images which are shared online through applications such as Flickr. Other historical locations can be associated to their geographic coordinates through Google Maps and visualized by means of applications like Google Street-View. Despite the place correspondence, the visual appearance of old and new images is dramatically different. As shown in Figure 1, ancient photographs have different colors, texture, and contrast characteristics compared to modern digital images [3]. Moreover it is not possible to control the acquisition perspective: changes in the urban planning along the years may have made some viewpoints not accessible.

Numerous efforts have been dedicated to recognizing landmarks in image databases containing photographs of the same era [4, 5, 6, 7], but to our knowledge, no previous work focused on tackling location recognition over large time lags. Here we



Figure 1: Pictures of four locations over large time lags showing an evident change in visual appearance. The photographs are similar in their high level scene content, but the color range and texture are significantly different. Modern photos can be easily found on the World Wide Web, while ancient pictures are provided by cultural heritage museums. The task we address in this paper consists in annotating ancient pictures given a set of labeled modern images.

define this task: **annotate an ancient photograph with the correct location label, given a set of labeled modern photos.** In particular, we propose several useful tools to cope with this problem, making three main contributions:

- we introduce a collection of images spanning over 25 locations and more than one century, with the eldest photographs dating back to the 1850s;
- we present a detailed analysis of existing feature representations, looking for the most robust features, suitable to handle the variability induced by different imaging processes adopted over time;
- old and new images can be considered as belonging to two different domains. We use existing domain adaptation meth-

\*Corresponding author

Email address: basura.fernando@esat.kuleuven.be (Basura Fernando)

<sup>1</sup>Telephone : +32163 72422

ods and we show promising results in both location recognition and interactive location retrieval.

The rest of the paper is organized as follows. Section 2 reviews the related work on location recognition and domain adaptation. Section 3 introduces our Large Time Lags Locations dataset and indicates the challenges of location recognition on this testbed. Section 4 briefly reviews the domain adaptation methods used in our study. In section 5 we present and discuss the obtained experimental results. Finally, section 6 concludes the paper and points out possible directions for future research.

## 2. Related Work

*Location recognition* consists in determining where a photo was taken by using as reference a database of previously seen locations [4]. The interest towards this task grew together with the number of freely available images on the Internet, many of which are geo-tagged and depict urban outdoor scenes. Today, with the widespread use of mobile devices endowed with built-in cameras and Internet connectivity, location recognition is a useful tool for city guides and smart navigation aids that are able to localize an image in near real time [8, 9].

Given a structured database covering a pre-defined set of places, location recognition can be tackled as a classification problem [5, 6]. The models for each place are learned offline and, at query time, a photograph is localized by assigning to it the label of the best scoring location classifier [5]. Previous work also considered this task as a retrieval problem: a query image is used to find a set of similar images from a database which are then returned as place suggestions [7, 10, 11]. This setting is mainly adopted when dealing with reference image collections possibly containing a large number of distractors.

Regardless of the chosen setup, one of the main challenges for location recognition is the choice of appropriate image descriptors. The variability in illumination conditions, viewpoint and occlusion can dramatically influence the similarity of images even depicting the same place or building. The data similarity is generally based on local descriptors and Bag-Of-Words (BOW) based techniques [12], and the retrieval is performed by computing distances between sparse BOW histograms [13]. Several improvements on this core system have been proposed by learning better descriptors [14, 15], introducing more accurate descriptor matching [16], exploiting 3D point clouds as powerful representations [4, 17], or carefully handling repetitive structures such as building facades [7].

The mentioned large visual variability occurs in spite of the standard practice of using photos acquired with high resolution modern cameras for location recognition. Although urban scenes and landmarks have been often captured even in ancient pictures and paintings, these samples are generally neglected and the further issues induced by vintage color processes or artistic brushstrokes are not considered in this task in the literature. One attempt to define robust detectors and descriptors was presented in [18, 19], where local symmetry features and spectral correspondence methods are proposed to match urban scenes with lighting, age and rendering style variations.

The problems of alignment between paintings and photographs [20, 21] and viewpoint re-capturing over time [22] have been tackled mainly leveraging over 3D models. The pioneering work of Shrivastava et al. [23] defined visual similarities between paintings and pictures taken in different seasons. The proposed method relies on the robustness of HOG features [24] and leverages the visual uniqueness of query images against millions of negative data. Despite their relevance, all these approaches have not been tested before for location recognition.

Solving the problem induced by data variability is also one of the goals of *domain adaptation* [25]. Instead of focusing directly on image-pairs matching, domain adaptation examines the data distributions from which the images are drawn. Specifically, two sets of data are considered as belonging to two different domains if they cover the same set of classes but their marginal distributions differ. The aim of domain adaptation is to reduce this distribution shift [25]. Various approaches fulfill this purpose by sample re-weighting and selection [26, 27], self-labeling [28, 29] and metric learning [30, 31]. A solution that has recently received a lot of attention in the computer vision community consists in embedding the samples in a low dimensional subspace shared by both the domains and invariant to their specific characteristics [32, 46, 33, 34]. This strategy allows to tackle cases where the samples present originally high dimensional feature vectors and one of the two domains contains only unlabeled samples (unsupervised domain adaptation).

Previous work demonstrated that time can naturally cause a visual domain shift [35, 36]. Existing methods applied to close this time gap proposed to discover object-specific style-sensitive patches [37], to predict the behavior of time-varying probability distributions [38] or to learn models adaptively over a continuous manifold [36]. However, all these approaches require details about the time ordering (evolution) of images, which is often difficult to obtain, especially with ancient photographs. In many cases only two set of data are available, one older than the other without any further information. Our work fits in this context. We focus on the problem of location recognition over large time lags where we are given a set of labeled modern photos and we want to annotate unlabeled historical pictures.

## 3. The Large Time Lags Locations Dataset

As detailed earlier, location recognition has so far been studied over modern images and the issues induced by large time lags have been only marginally considered for other tasks. Therefore one of the contributions of this paper is a database of images which spans over a wide time period and numerous locations. The dataset is presented in this section and used throughout the paper.

### 3.1. Details of the dataset

We introduce here our Large Time Lags Locations (LTLL) dataset containing pictures of 25 locations captured over a range of more than 150 years. Specifically, we collected images from

Image Set	minimum	maximum	mean
New Images	4	22	11
Old Images	1	22	8
Dataset	6	36	19

Table 1: Some dataset statistics. Minimum, maximum and mean number of images per class is shown.

several cities and towns in Europe such as Paris, London, Merelbeke, Leuven and ancient cities from Asia such as Agra in India, Colombo and Kandy from Sri Lanka. We chose thirteen locations considering the presence of well known landmarks for which it has been easy to download old and new pictures from the Web. The remaining twelve locations are in the municipality of Merelbeke, Flemish Province of East Flanders in Belgium. Ancient images of these historical locations dating back to the period 1850s-1950s have been provided by the city archive of Merelbeke. We downloaded the corresponding modern images from Flickr, Google Street-View and the Google Images search engine, although for some of the locations only a limited amount of modern photos could be obtained. Some statistics about the dataset is shown in Table 1.

In total the dataset contains 225 historical pictures and 275 modern ones. More details on the images and their metadata are available from our project web-page<sup>2</sup>.

### 3.2. Goals and Challenges

Our main goal is to recognize the location of an old picture using annotated modern photographs. Primarily, location recognition in this setting can be considered as an image classification task. In this paper we use the LTLL dataset to investigate the effectiveness of existing location recognition tools following the most typical image classification framework and using the standard pipeline with feature detection, description and encoding [39]. In comparison to previous location recognition benchmarks, the LTLL dataset poses new challenges related to the fact that the photos come from two different eras and to the limited amount of reference modern images for some historical place of cultural interest.

Given the LTLL dataset as testbed, we want to establish which of the existing feature detectors (Difference of Gaussians (DoG [40]), Hessian Affine [41], etc.), feature descriptors (SIFT, LIOP [42], etc.) and representations (BOW, Fisher Vectors [43], DeCAF [44]) is able to cope better with the image variability due to large time lags.

Due to variations in the capturing process as well as image degradation, old and new photographs belong to two different data distributions. Machine learning adaptive techniques are generally used in classification to overcome this kind of distribution mismatch issues. We investigate whether domain adaptation can help in reducing the distribution shift between old and new photographs in the LTLL database. We start our analysis by adopting a classification setup with the modern images

as training set (source) and the historical images as test samples (target). Apart from using all the images at once we also evaluate empirically the problems induced by the lack of modern data in the extreme case of having from one to five available training samples per location.

Finally, by combining the LTLL database with a large set of modern image distractors, we extend our study to cross-domain location retrieval. Here the ancient images are used as queries and the modern photos constitute the reference archive.

Before going into the details of the experimental analysis (provided in section 5), we dedicate the next section to a brief review of the considered domain adaptation methods.

## 4. Subspace Domain Adaptation

Among the existing domain adaptation approaches, we consider here three methods based on subspace learning. Most of the location recognition solutions rely on high dimensional features such as HOG or BOW with large vocabulary dimension of  $10^3 - 10^6$  words (see e.g. [5, 6]), and Fisher Vectors (FV, [43, 45]). Thus, using dimensionality reduction techniques appears to be a viable option. In the following we review the Geodesic Flow Kernel (GFK) method [33] and the Subspace Alignment (SA) approach [32] together with its Extended (ESA) version presented in [46]. All these domain adaptation methods are unsupervised: they operate directly on the data representation with the labels available only for the source domain. In the following subsections we specify the differences among them and the various strategies used to estimate the subspace dimensionality.

Let's indicate with  $x_S, x_T \in \mathbb{R}^{1 \times D}$  the samples belonging respectively to a *source* (training data, in our case new images which are labeled) and a *target* (testing data, in our case old images) domain. We assume to obtain the source domain subspace  $X_S \in \mathbb{R}^{D \times d_S}$ , and the target domain subspace  $X_T \in \mathbb{R}^{D \times d_T}$  by PCA, where  $d_S, d_T < D$  correspond to the number of selected eigenvectors associated with the largest eigenvalues.

### 4.1. GFK: Geodesic Flow Kernel

The GFK technique fixes the same dimensionality  $d = d_S = d_T$  for the subspaces of the two domains and embeds them onto a Grassmann manifold. The geodesic flow  $\{\Phi(t) : t \in [0, 1]\}$  between  $X_S = \Phi(0)$  and  $X_T = \Phi(1)$  is then used to parametrize the connection among the subspaces and to define infinitely many features varying gradually from the source to the target  $z^\infty = \{\Phi(t)^\top x : t \in [0, 1]\}$ . The inner product of the new features gives rise to a positive semidefinite kernel [33]

$$Sim(x_i, x_j) = \langle z_i^\infty, z_j^\infty \rangle = x_i^\top \int_0^1 \Phi(t)\Phi(t)^\top dt x_j = x_i \mathbf{G} x_j, \quad (1)$$

where the matrix  $\mathbf{G}$  can be calculated efficiently using singular value decomposition. The sample similarity obtained in this way is far less sensitive to the original domain differences. The dimensionality  $d$  is chosen by optimizing a *subspace disagreement measure* (SDM) that evaluates the similarity among the

<sup>2</sup><http://homes.esat.kuleuven.be/~bfernand/beeldcanon/>

source, the target and the combined source+target subspace. For more details, we refer to [33].

#### 4.2. SA: Subspace Alignment

The SA method learns a linear transformation matrix  $M \in \mathbb{R}^{d_S \times d_T}$  that aligns the source and target coordinate systems by minimizing the following Bregman divergence:

$$F(M) = \|X_S M - X_T\|_F^2, \quad (2)$$

where  $\|\cdot\|_F^2$  is the Frobenius norm. It can be easily shown that the optimal matrix is  $M = X_S' X_T$ , and the *target aligned source coordinate system* is  $X_a = X_S X_S' X_T$ . Finally, the similarity among two samples is defined as follows:

$$Sim(x_S, x_T) = (x_S X_a)(x_T X_T)'. \quad (3)$$

It is possible to demonstrate that the deviation between two successive eigenvalues is bounded [32]. The bound can be used to determine the maximum size of the subspaces  $d_{max}$  that allows to get a stable and non overfitting matrix  $M$ . The choice of the subspace dimensionality  $d$  can then be done by minimizing the classification error through a two fold *cross-validation* over the labeled source data and finally setting  $d_S = d_T = d$ . For more details, we refer the reader to [32].

#### 4.3. ESA: Extended Subspace Alignment

The function in (3) operates in the original  $\mathbb{R}^D$  space. However, after the domain transformation any problem can be formulated in the  $\mathbb{R}^{d_T}$  target subspace. To reduce the computational effort, ESA proposes to evaluate the similarity between the target aligned source samples and the target subspace projected data by using directly their Euclidean distance [46]:

$$\Theta(x_S, x_T) = \|x_S X_a - x_T X_T\|_2. \quad (4)$$

The cross-validation procedure described to define the best  $d$  for SA becomes very slow and tedious when working with data represented by high dimensional features. Moreover, it is unlikely to provide reliable results in cases where some source classes have an extremely limited number of annotated samples. When starting from a rich and reliable representation, one desideratum is to keep its strength and retain the sample local neighborhood after dimensionality reduction. With this purpose, ESA chooses the domain intrinsic dimensionality obtained through the method presented in [47]. The *Maximum Likelihood Estimate* (MLE) of the dimensionality for each data point is calculated and its average is used as the intrinsic dimensionality of the corresponding domain [46]. The two domains are considered separately, which implies  $d_S \neq d_T$ . For more details, we refer to [46].

## 5. Experiments

In this section we provide a detailed experimental analysis on the task of location recognition over large time lags using the new LTLL dataset introduced in section 3.

In the first part of the experiments, we use an image classification framework to evaluate different feature detectors, feature descriptors and image representations (section 5.1). Moreover, we investigate the advantages of using existing domain adaptation methods for the considered location recognition problem (section 5.2). All these tests are done using a Nearest Neighbor (NN) classifier. Given all the modern training images (source), each labeled with one of the 25 locations, we annotate a test ancient picture (target) with the location of the closest/most similar modern image. We use the standard Euclidean distance to evaluate the sample similarity unless specified otherwise, and equations (1), (3), (4) when applying the corresponding domain adaptation methods. The final performance is always evaluated by the multi-class classification accuracy obtained over the full set of old photographs. For this we calculate the percentage of correctly classified images over the full test images.

In the last part of our analysis, we study the task of cross-domain location retrieval and give details about the application of Extended Subspace Alignment (ESA) with relevance feedback (section 5.3). In this case we consider per-class average precision and take the mean average precision over all classes to obtain mAP. Several historical query images are accumulated together with their corresponding retrieved modern images. We show that by applying domain adaptation over them it is possible to learn a domain-invariant representation that provides a significant improvement in the mean average precision results.

### 5.1. Seeking The Best Image Representation

We start our experimental analysis by establishing which is the best image representation for the task of location recognition over large time lags, focusing on those that have been proposed as robust to large appearance changes. Most of them are obtained by the combination of local descriptors extracted from detected keypoints.

#### 5.1.1. Setup

We consider the following

**Detectors.** Among the existing detectors we test the Difference of Gaussians (**DoG** [40]), the Hessian Affine (**HA**, using the efficient implementation proposed in [41]), and a standard dense sampling strategy (**Dense**).

**Descriptors.** As descriptors we consider root-SIFT (**rSIFT**, [48]) and Local Intensity Order Pattern (**LIOP**, [42]).

**Representation.** Each image is represented either through Bag-of-Words (**BOW**), or Fisher Vectors (**FV**). In both cases the features are square-root and L2 normalized as suggested in [43].  $2 \times 10^5$  randomly sampled descriptors are used to build a 3000 visual word vocabulary with k-means, and to train a Gaussian mixture model (GMM). For FV we reduce the dimensionality of rSIFT and LIOP to 64 with PCA and we use a GMM with 64 components obtaining a final feature vector of dimension 8192.

We also evaluate features that have pre-defined detector-descriptor pairs.

318 *Self Similarity (Self-Sym [49]) and Symmetry Features (Sym-*  
 319 *Feat, [19]).* We follow the same procedure described before to  
 320 reduce the Self-Similarity descriptor dimension to 32 and combine  
 321 it with a GMM model with 128 components, maintaining  
 322 the final FV dimensionality of 8192.

323 *Edge Foci detector and Binary Coherent Edge descriptor (Edge-*  
 324 *Foci+BiCE, [50]).* This representation is described as robust  
 325 not only to illumination and pose changes, but also to intra-  
 326 category appearance variation. BiCE is a binary local descrip-  
 327 tor, so using a direct image-to-image matching procedure is  
 328 more natural and meaningful than passing through a BOW voc-  
 329 abulary or a GMM model for FV encoding. Two images are  
 330 matched by using the descriptors Hamming distance normal-  
 331 ized against the total number of extracted points, and compar-  
 332 ing the obtained value with a pre-defined threshold<sup>3</sup>.

333 Finally, we benchmark the classification results obtained with  
 334 the described representations against the performance of two  
 335 methods that have been previously applied on cross-domain  
 336 tasks. One is the approach presented in [23] based on the com-  
 337 bination of **HOG features and Exemplar SVM (ESVM, [51]).**  
 338 The other is the **NBNN classifier [52]**, considering its cross-  
 339 domain robustness discussed in [29].

340  
 341 We use *Acc. all* to indicate the accuracy obtained when  
 342 all new images are used for training a classifier with on average  
 343 eleven samples per location; *Acc. one* indicates instead the ac-  
 344 curacy obtained when a single (random) new photograph (per  
 345 class) is used in training. This last setup is quite challenging  
 346 due to lack of training samples. For it we report the average  
 347 classification accuracy and its standard deviation over 100 ran-  
 348 dom repetitions to get statistically meaningful results.

### 349 5.1.2. Analysis

350 All the recognition results are shown in Table 2, which is  
 351 divided in three parts. The first two are dedicated respectively  
 352 to BOW and FV with the NN classifier. The last part shows the  
 353 results obtained with the other considered representations and  
 354 classification methods.

355 With BOW the best performance is obtained when using  
 356 rSIFT as descriptor and a dense point extraction procedure. The  
 357 effect of the last one is evident in comparison with the corre-  
 358 sponding DoG-rSIFT and HA-rSIFT results. Due to the huge  
 359 difference in the visual appearance of old and new images the  
 360 interest points detected by DoG and HA loose their informative  
 361 power and it seems better to rely on a systematic sampling over  
 362 the whole image provided by the dense extraction. Moreover  
 363 LIOP presents very low performance, close to random, which  
 364 suggests that the relative order of pixel intensities in the de-  
 365 tected local patches changes significantly across the domains.

366 The symmetry information coded in the Sym-Feat descrip-  
 367 tors seems not preserved when passing from modern to old im-  
 368 ages, inducing low recognition results. On the other hand, Self-

Detec.	Descr.	Repr.	Class.	Acc. one (%)	Acc. all (%)
DoG	rSIFT	BOW	NN	7.5 ± 2.4	8.7
DoG	LIOP	BOW	NN	7.3 ± 3.5	7.7
Dense	rSIFT	BOW	NN	<b>19.9 ± 3.6</b>	<b>34.7</b>
Dense	LIOP	BOW	NN	6.3 ± 1.8	4.1
HA	rSIFT	BOW	NN	11.1 ± 3.1	17.9
HA	LIOP	BOW	NN	4.7 ± 1.9	9.2
Self-Sim		BOW	NN	15.8 ± 3.3	29.6
Sym-Feat		BOW	NN	6.1 ± 2.4	8.2
DoG	rSIFT	FV	NN	13.3 ± 2.2	20.9
DoG	LIOP	FV	NN	9.2 ± 1.5	16.3
Dense	rSIFT	FV	NN	22.7 ± 2.9	30.1
Dense	LIOP	FV	NN	4.9 ± 1.6	7.7
HA	rSIFT	FV	NN	<b>31.3 ± 3.5</b>	<b>48.5</b>
HA	LIOP	FV	NN	4.1 ± 1.5	4.6
Self-Sim		FV	NN	17.4 ± 2.8	33.7
Sym-Feat		FV	NN	14.0 ± 2.5	26.0
Edge-Foci	BiCE	Matching		10.7 ± 2.6	18.7
HOG		ESVM		15.9 ± 3.5	31.4
HA	rSIFT	FV	ESVM	<b>28.0 ± 3.4</b>	<b>44.6</b>
HA	rSIFT	NBNN		4.7 ± 1.0	7.1

Table 2: Comparison of detectors, descriptors, and image representations. We report the recognition rate results over the target (ancient) images in case of a single source (modern) sample per location (Acc. one), and when considering the full source set (Acc. all).

369 Similarity produces the second best results, showing the impor-  
 370 tance of mining the local geometric layout within each image  
 371 for cross-domain tasks.

372 The recognition rates obtained with FV are better on av-  
 373 erage than the corresponding ones based on BOW. The trend  
 374 among the different detector-descriptor cases is analogous to  
 375 what we discussed before, except that the HA detector appears  
 376 able to complement FV better than dense sampling, leading to  
 377 the highest performance. The disappointing results obtained  
 378 with Edge-Foci+BiCE indicate that this approach is clearly not  
 379 suitable for the task at hand.

380 The combination of HOG features and ESVM present a low  
 381 performance: as evident in the examples shown in Figure 2, the  
 382 HOG features mostly focus on the scene alignment, regardless  
 383 of the specific depicted location. As a variant we also combine  
 384 ESVM with HA-rSIFT-FV and the improved results underline  
 385 the importance of the feature representation. Still, compared to  
 386 a simple NN classifier, ESVM needs a set of extra negative sam-  
 387 ples besides the choice of learning parameters (i.e. tuning the  $C$   
 388 value), and does not yield better results. Finally the perfor-  
 389 mance of NBNN is almost random, indicating that for the con-  
 390 sidered task, the image-to-class paradigm is not strong enough  
 391 to overcome the difference among local descriptors in the train  
 392 and test set.

393 Overall the combination of HA detector, rSIFT descriptor  
 394 and FV encoding produces the best results and we will use this  
 395 representation for all the following experiments.

### 396 5.2. Domain Adaptation and Subspace Dimensionality

397 We investigate here the value of domain adaptation in clos-  
 398 ing the gap between historical and modern images. We test

<sup>3</sup>We tested different threshold values and we present here the best obtained result.



Figure 2: Examples of the results obtained with different feature representations and with ESA. Given the target test image in the first column, we show here the most similar source images. Red colour indicates wrongly classified instance whereas green indicates correctly classified instance. In the fifth and sixth rows only ESA correctly recognizes Notre Dame and Sacre Coeur. The last row shows a failure for all the methods. By comparing the columns it is visible that different features capture different levels of similarity with the query image and that HOG-ESVM mostly focus on the scene alignment.

399 the adaptive methods **GFK**, **SA** and **ESA**, comparing **SDM**<sub>408</sub>  
400 and **MLE** against other dimensionality estimation techniques,  
401 namely

402 **EIG**: the eigenvalue-based estimation is the standard solution  
403 used in the literature for which we choose the dimension-  
404 ality that retains 99% of the data variance.

405 **GMST**: the geodesic minimum spanning tree method [53] em-  
406 beds the data in a geodesic graph and prunes it to obtain-  
407 the graph spanning over all the samples with the mini-

mum total geodesic length.

409 **CDM**: the correlation dimension technique was proposed in  
410 [54] to approximate the fractal dimension of a dataset.

Note that the output of SDM is a single subspace dimension-  
ality value for both the domains while all the other methods  
provide two different values, one for each domain. We also re-  
mark that subspace learning is an unsupervised process, thus all  
the available samples can be used regardless of the availability  
of their class labels. We adopt the standard framework used in

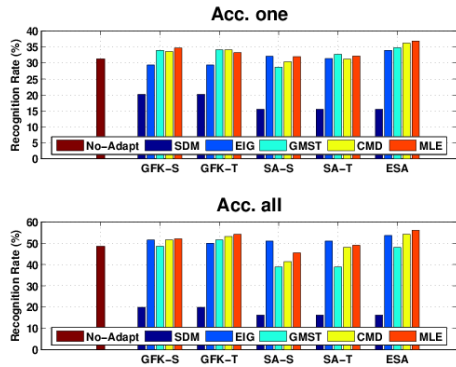


Figure 3: Nearest Neighbor classification results of several domain adaptation approaches (indicated in the x-axis) when changing the dimensionality estimation method (indicated in the legend). No-Adapt corresponds to using HA-rSIFT-FV representation without adaptation. -S and -T indicate that the dimensionality of the subspace was estimated on the source or on the target domain. For SDM, GFK-S=GFK-T and SA-S=SA-T. The title of the plot indicates that the results were obtained respectively with one sample per location (Acc. one) or considering the full source set (Acc. all) of modern images.

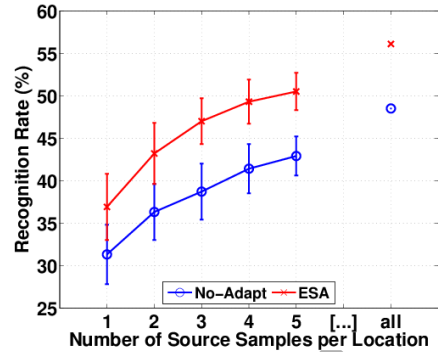


Figure 4: Nearest Neighbor classification performance obtained when changing the number of source samples per location. The results showed for 1 and “all” corresponds to what already shown in Figure 3 for ESA-MLE.

Method	Acc. one (%)	Acc. all (%)
DeCAF	36.3 ± 3.3	49.1
HA-rSIFT-FV	31.3 ± 3.5	48.5
HA-rSIFT-FV + ESA	36.9 ± 3.8	<b>56.1</b>
DeCAF + ESA	<b>39.3 ± 2.7</b>	49.0

Table 3: Classification rate obtained with different methods. The last row reports the best non-adaptive results of Table 2.

previous domain adaptation literature both for the adaptive and classification process. All modern training images are used to learn the source subspace  $X_S$  and all ancient testing images are used to learn target subspace  $X_T$ . We then rely on the labels of the source modern images (all or a subset depending on the experiment) to annotate the unlabeled test ancient photos. We report the classification accuracies in Figure 3.

From the histogram bars it can be immediately noticed that all the domain adaptation methods in combination with SDM produce worse results than No-Adapt which corresponds to using HA+rSIFT+FV and NN without adaptation (which we also reported in Table 2). This outcome is not so surprising if we consider that, from an original space dimensionality of 8192 the samples are projected to a subspace of dimension 16. All the other dimensionality estimation approaches provide higher values, for example EIG=199, GMST=49, CDM=56 and MLE=95 respectively. Even-though EIG is a simple technique, the classification accuracy is quite sensitive to the chosen energy percentages (99% in our experiments). Finally, MLE produces on average the best results with respect to all the other dimensionality estimation techniques.

When comparing the domain adaptation methods, we can see that ESA improves over all the other approaches. We also test ESA with MLE when varying the number of classifier training images between one and five: Figure 4 shows that even in the case of a reduced amount of labeled modern images this approach consistently improves over non adaptive classification.

Finally, to put our results in a wider perspective we add a further benchmark against the state of the art deep learning method. In the absence of large amount of training data, retraining a CNN network is prone to overfitting [55], and fine-tuning the last layers of an existing network does not converge not showing any meaningful learning. Thus we exploit directly the activation values of a pre-trained network as feature representation, namely DeCAF [56]. The results are reported in Table 3 together with what was originally achieved without

adaptation. We notice that ESA applied over FV outperforms what obtained with the DeCAF features [44]. However, when ESA is applied over DeCAF features, recognition rate obtained with one training sample (Acc. one (%)) seems to outperforms HA-rSIFT-FV + ESA. But when all training samples are used, HA-rSIFT-FV + ESA outperforms DeCAF + ESA. We conclude that in the task of location recognition over large time lags domain adaptation has a relevant impact with a particular advantage provided by ESA [46] over the other tested approaches.

### 5.3. Cross-Domain Location Retrieval

In this section we introduce the task of cross-domain location retrieval. Given a query old image showing a certain location, the goal is to retrieve modern images which depict the same location from a database (archive) consisting of few relevant images and large number of non-relevant images. Typical image retrieval databases contain  $10^4 - 10^6$  or more samples. To replicate this setting we enlarge our LTLL database by using images from the Oxford-building 105K database [48] obtaining a retrieval problem with 225 ancient query images and a modern image archive with 275 relevant images and 105K distractor images.

As an initial check, we adopt what is considered as best practice in standard instance retrieval [13, 48]. We use an image representation obtained by combining the Hessian Affine detector [41] with the root-SIFT [48] descriptor and BOW with a dictionary size of  $[10^4, 10^5, 10^6]$  created through an approximate k-means [13] and we use the tf-idf scheme. The performance obtained in this way is lower than what can be achieved with Fisher Vectors (see Table 4). A similar behavior can be observed with other interest point detectors, confirming what

we already discussed before in section 5.1. Motivated by the effectiveness of ESA to overcome the visual variability induced by large time lags in classification, we evaluate its extension to cross-domain location retrieval in the next section.

Method	mAP
BOW - 10K	0.123
BOW - 100K	0.122
BOW - 1M	0.086
Fisher Vectors	0.164

Table 4: Comparison of BOW and Fisher Vectors (FV parameters as in section 5.1) on cross domain location retrieval task using the LTL dataset and the Oxford-building 105K dataset as distractors. Old photographs are used as query images and the objective is to retrieve new images of the same location depicted in the query image.

### 5.3.1. Interactive Cross-Domain Retrieval With Domain Adaptation

Using domain adaptation in an instance retrieval setting turns out to be quite challenging. The reason is that domain adaptation relies on the samples of both the domains to learn and decompose the domain shift, but in image retrieval the query (target) samples are not available beforehand, while the source data (i.e. the subset of the database corresponding to relevant locations) can be identified only as more and more queries are issued. To overcome this lack of information we relax the problem and make the retrieval process interactive. The idea is to ask a user to select three relevant images from the retrieved result set of each query. By doing that we are able to collect some query images (old photographs or the target domain) and new relevant images (the source domain images). Finally, by using these collected samples we can estimate the subspaces of respective domains and use them to perform adaptation by learning the subspace alignment matrix  $M$  which is then used over new query images.

For the described process it is necessary to control the source and target sample cardinality: we need a minimum number of relevance feedback samples and queries to learn a full rank transformation matrix. We indicate with  $n_S^k$  the number of collected source images obtained with the feedback mechanism at round  $k$ , and with  $n_T^k$  the corresponding number of target query images. The respective subspace intrinsic dimensionalities  $\hat{d}_S$  and  $\hat{d}_T$  can be calculated by using 15 distinct images for each of the two domains: this amount of samples allows to evaluate 100 pairwise distances and provides enough information to set the local neighborhood of each sample for MLE [46]. The matrix  $M$  is then learned at the first iteration  $k = k^*$  which satisfies the conditions  $n_S^{k^*} > \hat{d}_S$  and  $n_T^{k^*} > \hat{d}_T$ . For our target task  $\hat{d}_T = 60$  and the source task  $\hat{d}_S = 95$ , so we collect 60 distinct queries and 180 feedbacks amounting to about 90-115 distinct modern images.

After the subspace alignment step over those data we also use PCA whitening [43] with the eigenvalues obtained from the query images. We repeat this experiment 10 times and we report the obtained mean average precision in Figure 5, together with the results obtained when increasing the number of query

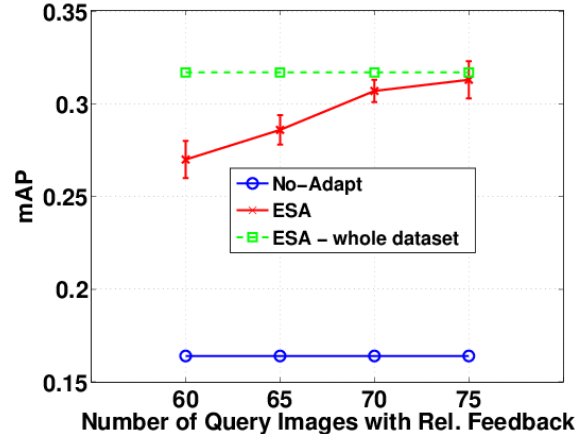


Figure 5: Retrieval results obtained when changing the number of query images. In this experiment the modern images are used as the reference database together with  $10^5$  distractors, while the old images are the queries. “No-Adapt” corresponds to the result obtained by using HA-rSIFT-FV without any adaptation. “ESA-whole dataset” refers to the result that can be obtained when the transformation matrix  $M$  is learned over the full set of old and new images of the 25 locations in our dataset. “ESA” indicates the interactive cross-domain retrieval method. We refer to the text for further details.

images. The plot shows that ESA outperforms the non adaptive solution and with 75 query samples it reaches almost the same results that would have been obtained by learning the transformation matrix  $M$  over our whole dataset (i.e. the same  $M$  used in the classification experiments). We also compare the obtained results with a naïve baseline method which exploits directly the similarity among the query images. Given a query sample we can first search the most similar image among the accumulated historical pictures and then use the associated modern feedback images to search in the modern archive. This procedure gives a mAp of  $0.201 \pm 0.023$ , which is still lower than what we obtained with ESA ( $0.313 \pm 0.010$ ).

Apart from being effective in the retrieval setting as shown, ESA makes the use of Fisher Vectors time and memory efficient since it operates in the low dimensional target space. In our experiments we need about 350Mb of RAM for 100K images and a single query is executed in less than 0.03 seconds using a single core of 2.8GHz. The matrix  $M$  can be learned in a few seconds, which allows ESA domain adaptation approach to be applied also in an online setup.

## 6. Conclusion

In this paper we introduced the task of recognizing the location depicted in an old photograph using modern digital images. We presented a dataset spanning over 25 locations and more than one century and we analyzed several representations looking for the most robust to the variability induced by color degradation and different image acquisition processes. Our experimental evaluation has shown that Hessian Affine detector [57, 41] and root-SIFT [48] in combination with Fisher Vectors [43] are more suitable for the task at hand than other detector-descriptor pairs originally introduced to cope with non-linear intensity changes [19, 50].

The difference in visual appearance among old and new images causes a domain shift at image descriptor level. Consequently, we obtain poor recognition performance for bag-of-words, descriptor matching approaches and NBNN. To overcome this problem we investigated the use of domain adaptation methods. Our analysis demonstrated that among different subspace adaptive learning approaches the Extended Subspace Alignment method [46] provides the best results and shows significant advantage in recognition over non-adaptive strategies (from 48.5% to 56.1%) and state-of-the-art CNN features [56] (49.1%).

Finally we proposed and analyzed the task of cross-domain location retrieval. We proposed a strategy to interactively use domain adaptation and showed the gain in performance provided by ESA also in this setting (from 0.201 to 0.313 mAP).

Our work presents several cues that indicate good directions for future research. We believe that the LTLL dataset introduced in this paper is a good testbed to evaluate the practical usefulness of existing domain adaptation methods. We plan to extend the collection and to investigate how adaptive methods scale in case of more samples and an increasing number of classes/locations. Indeed the application of domain adaptation on large datasets and the effect on their speed/complexity and accuracy have not been extensively studied yet. The proposed dataset may also influence the location recognition community to seek novel image representations that are not susceptible to distribution mismatch due to large time lags. Moreover our analysis suggests that there is a great necessity of new learning algorithms able to overcome the domain-shift issue in the cross-domain image retrieval setting. On one side the presented study paves the way for online-interactive domain adaptation systems, on the other it may inspire new instance retrieval methods and paradigms [58, 59].

**Acknowledgements** :The authors acknowledge the support of the EC FP7 project AXES and iMinds Impact project Beeldcanon.

## References

- [1] Venice time machine project, <http://vtm.epfl.ch/>.
- [2] Museum of london: Streetmuseum, <http://www.museumoflondon.org.uk/Resources/app/you-are-here-app/home.html>.
- [3] F. Palermo, J. Hays, A. A. Efros, Dating historical color images, in: European Conference on Computer Vision (ECCV), 2012.
- [4] Y. Li, N. Snavely, D. P. Huttenlocher, Location recognition using prioritized feature matching, in: European Conference on Computer Vision (ECCV), 2010.
- [5] P. Gronat, G. Obozinski, J. Sivic, T. Pajdla, Learning and calibrating place location classifiers for visual place recognition, in: International Conference on Computer Vision and Pattern Recognition (CVPR), 2013.
- [6] S. Cao, N. Snavely, Graph-based discriminative learning for location recognition, in: International Conference on Computer Vision and Pattern Recognition (CVPR), 2013.
- [7] A. Torii, J. Sivic, T. Pajdla, M. Okutomi, Visual place recognition with repetitive structures, in: International Conference on Computer Vision and Pattern Recognition (CVPR), 2013.
- [8] H. Altwaijry, M. Moghimi, S. Belongie, Recognizing locations with google glass: A case study, in: IEEE Winter Conference on Applications of Computer Vision (WACV), 2014.
- [9] T. Chen, K. Wu, K. Yap, Z. Li, F. S. Tsai, A survey on mobile landmark recognition for information retrieval, in: International Conference on Mobile Data Management (MDM), 2009.
- [10] G. Schindler, M. Brown, R. Szeliski, City-scale location recognition, in: International Conference on Computer Vision and Pattern Recognition (CVPR), 2007.
- [11] X. Li, C. Wu, C. Zach, S. Lazebnik, J.-M. Frahm, Modeling and recognition of landmark image collections using iconic scene graphs, in: European Conference on Computer Vision (ECCV), 2008.
- [12] J. Sivic, A. Zisserman, Video google: A text retrieval approach to object matching in videos, in: International Conference on Computer Vision (ICCV), 2003.
- [13] J. Philbin, O. Chum, M. Isard, J. Sivic, A. Zisserman, Object retrieval with large vocabularies and fast spatial matching, in: International Conference on Computer Vision and Pattern Recognition (CVPR), 2007.
- [14] C. Doersch, S. Singh, A. Gupta, J. Sivic, A. A. Efros, What makes paris look like paris?, in: SIGGRAPH, 2012.
- [15] J. Philbin, M. Isard, J. Sivic, A. Zisserman, Descriptor learning for efficient retrieval, in: European Conference on Computer Vision (ECCV), 2010.
- [16] H. Jegou, M. Douze, C. Schmid, Hamming embedding and weak geometric consistency for large scale image search, in: European Conference on Computer Vision (ECCV), 2008.
- [17] T. Sattler, B. Leibe, L. Kobbelt, Fast image-based localization using direct 2d-to-3d matching, in: International Conference on Computer Vision (ICCV), 2011.
- [18] M. Bansal, K. Daniilidis, Joint spectral correspondence for disparate image matching, in: International Conference on Computer Vision and Pattern Recognition (CVPR), 2013.
- [19] D. C. Hauagege, N. Snavely, Image matching using local symmetry features., in: International Conference on Computer Vision and Pattern Recognition (CVPR), 2012.
- [20] M. Aubry, B. Russell, J. Sivic, Painting-to-3d model alignment via discriminative visual elements, Tech. rep., INRIA (2013).
- [21] B. C. Russell, J. Sivic, J. Ponce, H. Dessales, Automatic alignment of paintings and photographs depicting a 3d scene, in: 3dRR, 2011.
- [22] S. Bae, A. Agarwala, F. Durand, Computational rephotography, ACM Trans. Graph. 29 (3) (2010) 24:1–24:15.
- [23] A. Shrivastava, T. Malisiewicz, A. Gupta, A. A. Efros, Data-driven visual similarity for cross-domain image matching, in: SIGGRAPH ASIA, 2011.
- [24] N. Dalal, B. Triggs, Histograms of oriented gradients for human detection, in: International Conference on Computer Vision and Pattern Recognition (CVPR), 2005.
- [25] J. Jiang, A literature survey on domain adaptation of statistical classifiers, Available from: [http://sifaka.cs.uiuc.edu/jiang4/domain\\_adaptation/survey/da\\_survey.html](http://sifaka.cs.uiuc.edu/jiang4/domain_adaptation/survey/da_survey.html) (2008).
- [26] J. J. Lim, R. Salakhutdinov, A. Torralba, Transfer learning by borrowing examples for multiclass object detection, in: Advances in Neural Information Processing Systems (NIPS), 2011.
- [27] B. Gong, K. Grauman, F. Sha, Connecting the dots with landmarks: Discriminatively learning domain-invariant features for unsupervised domain adaptation, in: International Conference on Machine Learning (ICML), 2013.
- [28] L. Bruzzone, M. Marconcini, Domain adaptation problems: A dasvm classification technique and a circular validation strategy, IEEE Transactions on Pattern Analysis and Machine Intelligence (TPAMI) 32 (5) (2010) 770–787.
- [29] T. Tommasi, B. Caputo, Frustratingly easy nbnn domain adaptation, in: International Conference on Computer Vision (ICCV), 2013.
- [30] B. Kulis, K. Saenko, T. Darrell, What you saw is not what you get: Domain adaptation using asymmetric kernel transforms, in: International Conference on Computer Vision and Pattern Recognition (CVPR), 2011.
- [31] K. Saenko, B. Kulis, M. Fritz, T. Darrell, Adapting visual category models to new domains, in: European Conference on Computer Vision (ECCV), 2010.
- [32] B. Fernando, A. Habrard, M. Sebban, T. Tuytelaars, Unsupervised visual domain adaptation using subspace alignment, in: International Conference on Computer Vision (ICCV), 2013.
- [33] B. Gong, Y. Shi, F. Sha, K. Grauman, Geodesic flow kernel for unsupervised domain adaptation, in: International Conference on Computer

- 689 Vision and Pattern Recognition (CVPR), 2012. 760
- 690 [34] R. Gopalan, R. Li, R. Chellappa, Domain adaptation for object recogni-761  
691 tion: An unsupervised approach, in: International Conference on Com-762  
692 puter Vision (ICCV), 2011. 763
- 693 [35] K. Rematas, B. Fernando, T. Tommasi, T. Tuytelaars, Does evolution764  
694 cause a domain shift?, in: International Workshop on Visual Domain765  
695 Adaptation and Dataset Bias (VisDA-ICCV), 2013. 766
- 696 [36] J. Hoffman, T. Darrell, K. Saenko, Continuous manifold based adaptation767  
697 for evolving visual domains, in: International Conference on Computer  
698 Vision and Pattern Recognition (CVPR), 2014.
- 699 [37] Y. J. Lee, A. A. Efros, M. Hebert, Style-aware mid-level representation  
700 for discovering visual connections in space and time, in: International  
701 Conference on Computer Vision (ICCV), 2013.
- 702 [38] C. H. Lampert, Predicting the future behavior of a time-varying probabil-  
703 ity distribution (2014). [arXiv:http://arxiv.org/abs/1406.](http://arxiv.org/abs/1406.5362)  
704 [5362](http://arxiv.org/abs/1406.5362).
- 705 [39] K. Chatfield, V. Lempitsky, A. Vedaldi, A. Zisserman, The devil is in  
706 the details: an evaluation of recent feature encoding methods, in: British  
707 Machine Vision Conference (BMVC), 2011.
- 708 [40] D. Marr, E. Hildreth, Theory of edge detection, *Proceedings of the Royal  
709 Society of London Series B* 207 (1980) 187–217.
- 710 [41] M. Perdoch, O. Chum, J. Matas, Efficient representation of local ge-  
711 ometry for large scale object retrieval, in: International Conference on  
712 Computer Vision and Pattern Recognition (CVPR), 2009.
- 713 [42] Z. Wang, B. Fan, F. Wu, Local intensity order pattern for feature descrip-  
714 tion, in: International Conference on Computer Vision (ICCV), 2011.
- 715 [43] F. Perronnin, J. Sánchez, T. Mensink, Improving the fisher kernel for  
716 large-scale image classification, in: European Conference on Computer  
717 Vision (ECCV), 2010.
- 718 [44] J. Donahue, Y. Jia, O. Vinyals, J. Hoffman, N. Zhang, E. Tzeng, T. Dar-  
719 rell, Decaf: A deep convolutional activation feature for generic visual  
720 recognition, in: International Conference on Machine Learning (ICML),  
721 2014.
- 722 [45] T. Jaakkola, D. Haussler, Exploiting generative models in discrimina-  
723 tive classifiers, in: *Advances in Neural Information Processing Systems*  
724 (NIPS), 1998.
- 725 [46] B. Fernando, A. Habrard, M. Sebban, T. Tuytelaars, Subspace align-  
726 ment for domain adaptation, *arXiv preprint arXiv:1409.5241* (2014) 1–  
727 20. [arXiv:http://arxiv.org/abs/1409.5241](http://arxiv.org/abs/1409.5241).
- 728 [47] E. Levina, P. J. Bickel, Maximum likelihood estimation of intrinsic  
729 dimension., in: *Advances in Neural Information Processing Systems*  
730 (NIPS), 2004.
- 731 [48] R. Arandjelovic, A. Zisserman, Three things everyone should know to im-  
732 prove object retrieval, in: International Conference on Computer Vision  
733 and Pattern Recognition (CVPR), 2012.
- 734 [49] E. Shechtman, M. Irani, Matching local self-similarities across images  
735 and videos, in: International Conference on Computer Vision and Pattern  
736 Recognition (CVPR), 2007.
- 737 [50] C. L. Zitnick, Binary coherent edge descriptors, in: European Conference  
738 on Computer Vision (ECCV), 2010.
- 739 [51] T. Malisiewicz, A. Gupta, A. A. Efros, Ensemble of exemplar-svm for  
740 object detection and beyond, in: International Conference on Computer  
741 Vision (ICCV), 2011.
- 742 [52] O. Boiman, E. Shechtman, M. Irani, In defense of nearest-neighbor based  
743 image classification., in: International Conference on Computer Vision  
744 and Pattern Recognition (CVPR), 2008.
- 745 [53] J. Costa, A. O. Hero, Manifold learning with geodesic minimal spanning  
746 trees, in: *CoRR*, 2003. [arXiv:http://arxiv.org/abs/cs.CV/](http://arxiv.org/abs/cs.CV/0307038)  
747 [0307038](http://arxiv.org/abs/cs.CV/0307038).
- 748 [54] G. P. Decoster, D. W. Mitchell, The efficacy of the correlation dimension  
749 technique in detecting determinism in small samples, *Journal of Statistical  
750 Computation and Simulation* 39 (4) (1991) 221–229.
- 751 [55] J. Hoffman, E. Tzeng, J. Donahue, Y. Jia, K. Saenko, T. Darrell, One-shot  
752 adaptation of supervised deep convolutional models, in: *CoRR*, 2013.  
753 [arXiv:http://arxiv.org/abs/1312.6204](http://arxiv.org/abs/1312.6204).
- 754 [56] A. S. Razavian, H. Azizpour, J. Sullivan, S. Carlsson, CNN Features  
755 off-the-shelf: an Astounding Baseline for Recognition (2014). [arXiv:](http://arxiv.org/abs/1403.6382)  
756 [1403.6382](http://arxiv.org/abs/1403.6382).
- 757 [57] K. Mikolajczyk, T. Tuytelaars, C. Schmid, A. Zisserman, J. Matas,  
758 F. Schaffalitzky, T. Kadir, L. Van Gool, A comparison of affine region de-  
759 tectors, *International Journal of Computer Vision (IJCV)* 65 (1-2) (2005)  
43–72.
- [58] B. Fernando, T. Tuytelaars, Mining multiple queries for image retrieval:  
On-the-fly learning of an object-specific mid-level representation, in: In-  
ternational Conference on Computer Vision (ICCV), 2013, pp. 2544–  
2551.
- [59] R. Arandjelovic, A. Zisserman, Multiple queries for large scale specific  
object retrieval., in: British Machine Vision Conference (BMVC), 2012,  
pp. 1–11.